Lab on a Chip

Cite this: *Lab Chip*, 2012, **12**, 2719–2725

www.rsc.org/loc

PAPER

Wafer-scale mitochondrial membrane potential assays†

Tae-Sun Lim,‡[a] Antonio Davila Jr,‡[bc] Katayoun Zand,[a] Douglas C. Wallace[c] and Peter J. Burke[a]

Received 23rd January 2012, Accepted 25th April 2012
DOI: 10.1039/c2lc40086c

It has been reported that mitochondrial metabolic and biophysical parameters are associated with degenerative diseases and the aging process. To evaluate these biochemical parameters, current technology requires several hundred milligrams of isolated mitochondria for functional assays. Here, we demonstrate manufacturable wafer-scale mitochondrial functional assay lab-on-a-chip devices, which require mitochondrial protein quantities three orders of magnitude less than current assays, integrated onto 4′′ standard silicon wafer with new fabrication processes and materials. Membrane potential changes of isolated mitochondria from various well-established cell lines such as human HeLa cell line (Heb7A), human osteosarcoma cell line (143b) and mouse skeletal muscle tissue were investigated and compared. This second generation integrated lab-on-a-chip system developed here shows enhanced structural durability and reproducibility while increasing the sensitivity to changes in mitochondrial membrane potential by an order of magnitude as compared to first generation technologies. We envision this system to be a great candidate to substitute current mitochondrial assay systems.

1 Introduction

The mitochondrial membrane potential ($\Delta\psi_m$) plays a crucial role in the production of ATP as an energy source of the cell. The electron transport chain (complex I, II, III, IV) positioned at the mitochondrial inner membrane generates this electrochemical potential gradient across the inner membrane by pumping protons through the mitochondrial inner membrane while sequentially transporting electrons through the complexes. This proton gradient is utilized by ATP synthase (complex V) to synthesize ATP from ADP and inorganic phosphate. This cycle can remain functional and constantly produce ATP to sustain the cell only when the electrochemical proton gradient is maintained at a constant level with enough available ADP. $\Delta\psi_m$ is the key component of this electrochemical potential gradient, therefore it is important to develop instrumentation technologies to monitor $\Delta\psi_m$ in order to efficiently evaluate mitochondrial function.[1]

Mitochondria are known to regulate cell life and death by control of apoptosis, through a critical, irreversible step involving the mitochondrial permeability transition pore (mPTP), a mega-pore complex triggered to open under certain conditions at both the mitochondrial inner and outer membranes.[2–7] Once opened, the permeability of the mitochondrial inner membrane increases drastically, causing the release of bioactive proteins including cytochrome C and the inflow of protons, resulting in an irreversible collapse of the mitochondrial membrane potential. This process is known to lead to apoptosis. In addition, malfunctions and abnormal behaviors of mitochondria are highly associated with the degenerative diseases and the aging process.[8–10]

A lipophilic cation such as tetraphenylphosphonium (TPP^+) diffuses through the mitochondrial inner membrane, the concentration ratio depending on $\Delta\psi_m$, determined by the Nernst equation, *i.e.*

$$\frac{[TPP^+]_{out}}{[TPP^+]_{in}} = e^{\frac{\Delta\Psi_m}{kT}} \quad (1)$$

By measuring the concentration of TPP^+ outside the mitochondria,$[TPP^+]_{out}$, using electrochemical ion selective electrode technology, one can infer the concentration of cation taken up into the mitochondria,$[TPP^+]_{in}$, to determine the membrane potential.[7] Previously, we reported on an electrochemical mitochondrial functional assay using a miniaturized on-chip mitochondrial membrane potential sensor equipped with TPP^+ ion selective electrodes.[11] This first generation planar-type mitochondrial assay sensor showed good sensitivity and a fast response to $\Delta\psi_m$ by monitoring the activity of TPP^+ in the sample solution. However, there were some challenges with the construction process and other factors that could limit the use of the sensor. First, the ion selective membrane was manually cut

[a]*Integrated Nanosystem Research Facility, Electrical Engineering and Computer Science, University of California, Irvine, CA, USA*
[b]*Center for Molecular and Mitochondrial Medicine and Genetics, Department of Biological Chemistry, University of California, Irvine, CA, USA*
[c]*Center for Mitochondrial and Epigenomic Medicine, Children's Hospital of Philadelphia, University of Pennsylvania, Philadelphia, PA, USA*
† Electronic supplementary information (ESI) available. See DOI: 10.1039/c2lc40086c
‡ These authors contributed equally to this work.

from a thin jelly membrane sheet on the glass substrate itself and then individually transferred onto an open trench of PDMS layers. This was laborious and often caused wrinkles resulting in weak bonding between the membrane and the PDMS layer and, subsequently, electrolyte leakage. This could lead to unstable sensor performance and a shorter sensor lifetime. In order to improve the production yield, we sought to evolve our fabrication approaches with new substrate materials to replace the manual, serially fabricated single sensor built upon a microscope slide with an efficient batch, parallel fabrication process based on semiconductor industry models.

Here, we demonstrate a second generation, wafer-scale lab-on-a-chip design and fabrication process for mitochondrial bioenergetic measuring which is compatible with microfabrication technology. This product is much more efficient to produce and proves to have significantly higher reproducibility and durability than the first generation model. We use industry standard 4′′ silicon wafer as the substrate along with a new membrane transfer technique. Changes in the mitochondrial membrane potential of isolated mitochondria from the established human cell lines Heb7A and 143B and from mouse muscle tissue are evaluated in response to treatments with known modulators of mitochondrial function. The sensor is validated by taking the measured TPP^+ concentration, converting into $\Delta\psi_m$ and calibrating against the theoretical values. This latest sensor model improves upon all of the functional parameters of the previous version, is capable of higher throughput analysis and, importantly, is much more time and cost-effective to fabricate. This lays the foundation for low cost, high throughput screening of bioenergetics and metabolism in an on-chip format.

2 Methods

Fabrication steps

The microfabrication process is schematically depicted in Fig. 1. A 4′′ bare silicon wafer (Boron doped P-type) was used as the device substrate to allow compatibility with standard semiconductor wafer-scale microfabrication technologies. The wafers were treated with boiling piranha solution (3 : 1 = sulfuric acid: DI water) for an hour followed by an organic solvent clean, then rinsed with copious DI water. Thin films of Ti (50 nm) and Ag (1.5 μm) were deposited using e-beam evaporation. The silver film was lithographically patterned into electrodes using Shipley 1827 photoresist (Fig. 1 (a)). Wet etching was carried out using a silver etchant made of 1 : 1 mixture of nitric acid and DI water followed by Ti etching. The patterned silver electrodes were chlorinated chemically by dropping 50 μl of 0.1 M $FeCl_3$ solutions onto the electrode area, situated within the inner

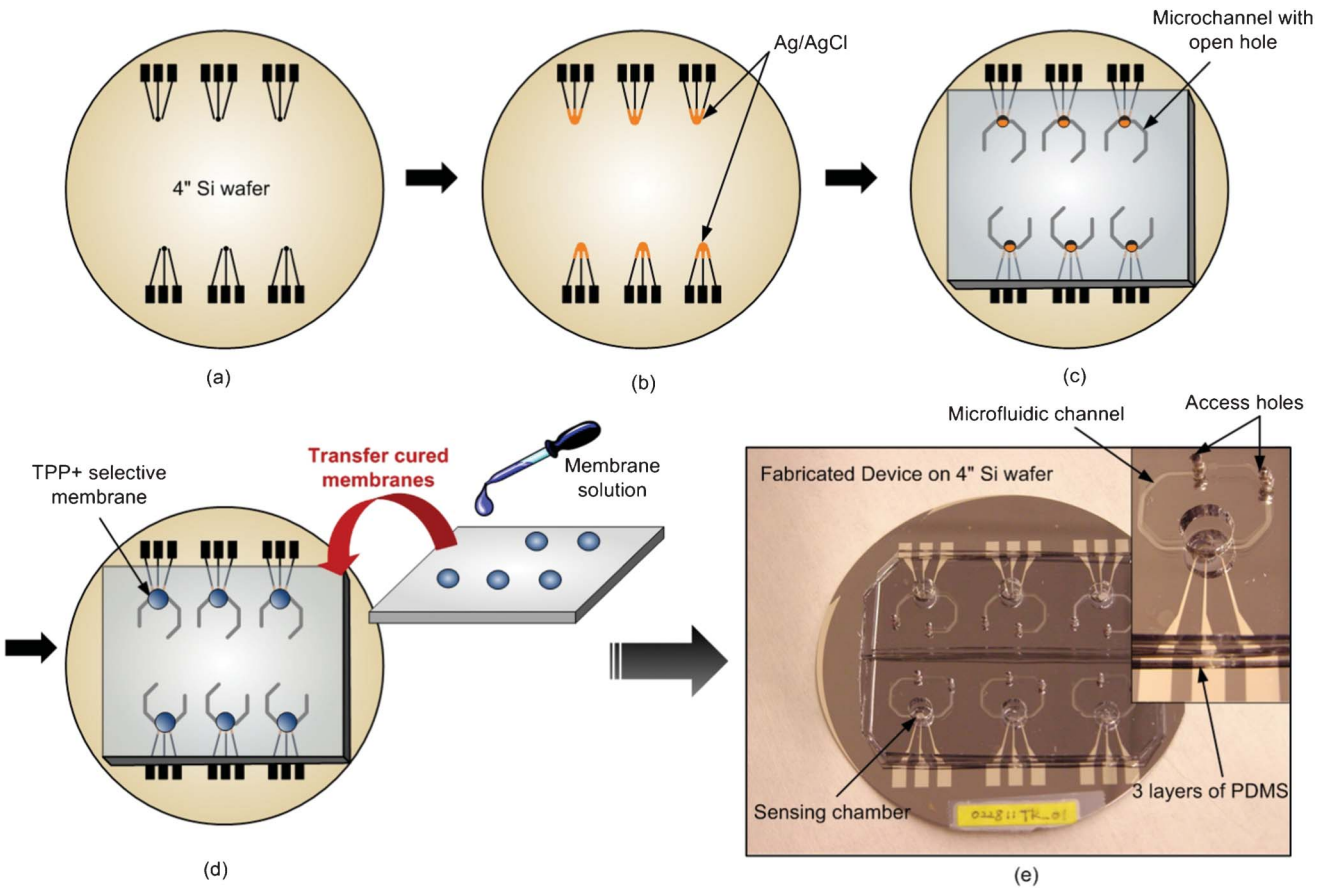

Fig. 1 Schematic diagrams of microfabrication steps and the fabricated device. (a) Silver thick film deposition and patterning into electrode arrays on a 4′′ Si wafer. (b) Chlorination of silver to make Ag/AgCl on the sensing areas. (c) Assembly of the 1st PDMS layer with microfluidic channels. (d) TPP^+ selective membrane transfer by flipping over the thin PDMS layer with cured membranes. (e) Photograph of the constructed device (inset, showing a sensing chamber and access holes) and one complete set of six sensors manufactured in a batch, parallel process on a single 4′′ Si wafer.

electrolyte chamber, for 40 s at room temperature to create Ag/AgCl electrodes (Fig. 1 (b)). Three layers of silicone rubber (PDMS) were prepared separately by soft lithography. The first layer has a microfluidic channel (400 μm × 50 μm) to contain the 10 mM TPP^+ inner filling solution needed for the ion selective sensing. These microfluidic channels were produced by soft lithography with a thick negative photo resist (SU-8) mold to keep the volume of the inner filling solution constant compared to the hand-cut L-shaped reservoirs from our previous reported sensor (Fig. 1 (c)). A 2 mm hole was drilled through the center of the microfluidic channel to provide an interface between the inner filling solution and the medium in the sensing chamber through the ion selective membrane. The TPP^+ ion selective (IS) membrane solution was prepared with a mixture of 4.4 mL of tetrahydrofuran (THF) and dioctyl phthalate, 0.15 g of polyvinyl chloride (PVC), and 6 mg of precipitation of tetraphenylboron (Na^+TBP^-)[12], and transferred onto a PDMS layer by a new transfer technique (described below). To streamline the fabrication process, we utilized a commercial, leakage-free Ag/AgCl reference electrode (Warner Instruments) and fabricated only the working electrode with the IS membrane.

In order to create reproducible membranes and ensure their secure, wrinkle-free bonding with the underlying PDMS layer, we developed a transfer method in which the IS membranes are first prepared and cured on a separate PMDS scaffold before being positioned and deposited on the chip. As depicted in Fig. 1 (d), a clean 2 mm thick PDMS scaffold was first aligned atop the first PDMS layer, such that the open 2 mm center holes of six microfluidic channels are visible from above. 30 μL of freshly prepared ion selective membrane solution was then carefully dropped onto the scaffold to correspond to the position of the channel holes underneath. These were allowed to cure overnight at room temperature. The following day, the scaffold was flipped over, carefully positioned so the cured IS membranes fell within the chamber holes, and gently pressed out for 5–10 min. This resulted in intact IS membranes that were completely and accurately transferred into position without wrinkles. We also tried this transfer method at elevated temperature (~ 60 °C) in a hot oven, assuming that the membrane would be more pliable and allow for easier transfer. Although the transfer was successful, we found that the high-temperature treated membranes did not exhibit proper responses to changes in [TPP^+]. We believe this is because the sensitivity of the IS membrane is a non-linear function of temperature (data not shown). The remaining two PDMS layers were aligned and assembled together manually under a stereomicroscope. The bottom microfluidic channel was filled with 10 mM TPP^+ through the access holes using a micropipette. The completed mitochondrial lab-on-a-chip device in Fig. 1 (e) shows an array of 6 fully manufactured sensors, with three layers of PDMS constructed on a 4″ silicon wafer. The inset reveals the components of the chip including the bottom microfluidic channel with its access holes and the open 80 μL circular sensing chamber.

To summarize, the advantages of this second generation technology over the first generation include 1) A Si 4″ wafer process (rather than microscope slides), 2) Lithographically defined PDMS microfluidic channels (as opposed to hand cut), 3) Batch compatible, transfer process for membrane assembly (rather than manual membrane glue in place), and 4) A batch, completely automatable, parallel manufacturing process that can be scaled up to multiple devices per wafer) as opposed to manual, serial assembly of each device component by component. We now turn to the performance of the improved devices.

Results and Discussion

Characterization

The experimental set-up for the sensor calibration and measurement is shown in Fig. 2. One of the patterned working electrodes (Ag/AgCl) was connected to a digital multimeter (Agilent 34401A, input impedance setting = 10 GΩ) along with a commercial leakage-free Ag/AgCl reference electrode (Warner Instruments). A computer installed with LabView was linked to the digital multimeter for data acquisition *via* a GPIB interface (National Instrument, GPIB-USB-HS). The acquired data was analyzed and plotted using Igor Pro (WaveMetrics).

The sensor was primed for use by filling the sensing chamber and underlying microfluidic chamber with 10 mM TPP^+ solution overnight to activate the TPP^+ IS membrane. The next day, the inner filling solution was replaced with care taken to prevent bubble formation which could create an open circuit against the IS membrane and signal-reading errors. The sensing chamber was rinsed with DI water and respiration buffer (refer to supplemental information for composition) 3 times before filling with fresh respiration buffer. The sensor was extensively characterized using a 5-point calibration curve with TPP^+ concentrations ranging from 0.3 μM to 600 μM. The potential difference between the reference and working electrodes was monitored while incrementally increasing the TPP^+ concentrations within the sensing chamber.

Fig. 2 (c) shows two calibration curves measured before and after a typical mitochondrial measurement (see below) and demonstrates the sensors reproducibility, durability, and small drift between experiments. The insert plot shows the signal stabilizing just a few seconds following each successive addition of TPP^+ (arrows) which marks a 60% faster response time compared with our original sensor without its tapering large signal spikes. TPP^+ concentrations were plotted logarithmically to reveal the linear relationship between concentration and IS electrode (ISE) potential (mV) as predicted by the Nernst equation. Since our experimental concentration range is between 5 and 10 μM, we typically perform a 2-point curve fit between our 2nd and 3rd calibration points (3 μM and 30 μM respectively). These measurements of ISE potential were used to determine sensor variation using the following equation:

$$(V_{ISE} = J * ln[TPP^+]+K), \quad (2)$$

where V_{ISE} is the measured ISE potential, and J and K are the two calibration coefficients.

An important issue is the statistical variation among sensors, which we now address. Fig. 2 (d) illustrates the statistical data from 21 separate calibration curves performed on eight different devices. The J and K coefficients of variation represent the ratio of the standard deviations to the averages which, in our hands, resulted in values of ≈ 18% and ≈ 16%, respectively. This includes the effects of *both* device-to-device variations, as well as variations from run-to-run within one device. This narrow data distribution indicates

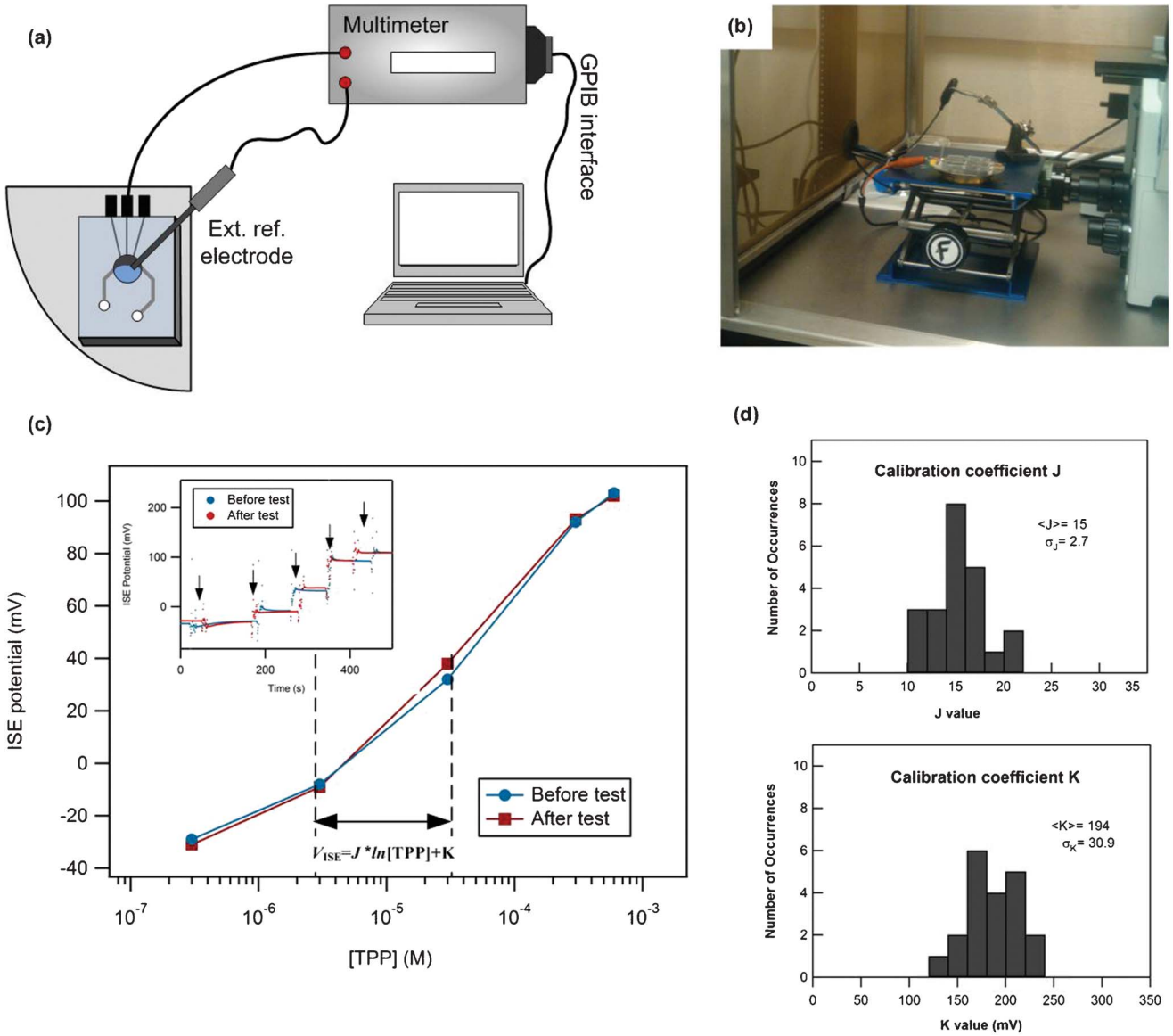

Fig. 2 (a) Schematic of experimental set-up showing the sensing chamber, the sensor connected to the external reference electrode, and one of the electrode pads connected to a multimeter which is linked to a computer installed with Lab View for data acquisition. (b) Photograph set-up. (c) 5-point calibration curves performed before/after mitochondrial assays showing reproducibility of the sensor. The slope of the highlighted area was used for data conversion (Inset: time trace of ISE potential response during the calibration, arrows showing additions of TPP^+.) (d) Statistical variation of J and K values from 21 separate calibrations from 8 separate devices.

good reproducibility of the sensor response and a small device-to-device variation. This is an improvement over our previous devices[15] where the slope and offset from both sources of error (device-to-device and run-to-run) varied by a much larger amount, specifically ≈ 25% and ≈ 82% for J and K equivalent, respectively, and indicates the significance of developing a wafer scale manufacturing process. While excellent, this variation in calibration coefficients may still require a careful calibration before each measurement for some envisioned assays that require high accuracy, an issue we hope to address in future generations of our chips.

Mitochondrial membrane potential measurement

As a demonstration with known cell lines, a mitochondrial membrane potential assay was performed in respiration buffer at room temperature using isolated mitochondria prepared from human cell lines, including Heb7A and 143B TK-, and also from mouse liver (Isolation protocols given in supplemental information). During the measurement, the isolated mitochondria were maintained on ice to prevent degradation. For each individual sample, the TPP^+ concentration traces were monitored before and after the addition of mitochondria to establish a basal "resting" potential. Then, changes in the mitochondrial membrane potential were recorded as OXPHOS complex I substrates (pyruvate and malate) and ADP were added to the sensor chamber. These measurements were converted to membrane potential using a procedure similar to our previous publication[11] (discussed in supplemental information).

In order to allow for improved quantitative measurements of the membrane potential of various cell lines, we developed a

procedure in which all of the initial starting concentrations and volume of solution and mitochondria were the same from experiment to experiment, the only variable being the cell line that produced the mitochondria. We chose an initial concentration of 7.2 μM for all the experiments, allowing for the same initial starting point (prior to the introduction of mitochondria) for all experiments. Using this technique, the initial value of TPP^+ was always known, and only changes in TPP^+ were needed. Thus, for the calibration, only the logarithmic slope of the TPP^+ *vs.* V_{ISE} curve was important. In an experiment where the TPP^+ *vs.* V_{ISE} curve was measured immediately before and immediately after the experiment, the values of J changed by ~ 15% (20.8 *vs.* 17.5 mV for J). In our experiments, we used only the logarithmic slope (J^{-1}) to determine the value of TPP^+ after introduction of the mitochondria. More on the error analysis will be presented below.

A representative result from a mitochondrial membrane potential experiment is shown in Fig. 3 with $[TPP^+]$ values obtained from the calibration curve conversion. After adjusting the chamber working concentration of TPP^+ to 7.2 μM, 5 μL of 150 ng μL^{-1} freshly isolated mitochondria were introduced into the 80 μL sensing chamber. Our experimental working concentration, 10 ng μL^{-1}, is three orders of magnitude less than is needed by conventional assays.[12,13] The chamber solutions were mixed gently three times using a micropipette and the trace was allowed to stabilize and remain constant showing that the solution is thoroughly mixed and no further diffusion occurred due to the incomplete mixing during the measurement (data not shown). Upon introduction of mitochondria, mitochondria quickly absorbed TPP^+ according to their $\Delta\psi_m$ leading to decrease in $[TPP^+]$ in the sensing chamber.

In our experiments, the addition of 5 μL of solution containing mitochondria would lower the TPP^+ concentration (even in the absence of mitochondria) by about 0.5 μM. Because of the membrane potential, there is an additional reduction in $[TPP^+]$

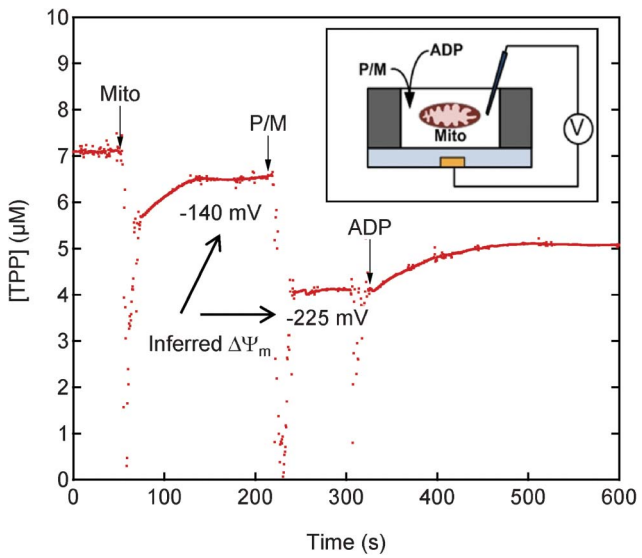

Fig. 3 Measurement of $[TPP^+]$ with isolated mitochondria from 143B TK- osteosarcoma cells. Vertical arrows indicate successive addition of 5 μL of 150 ng μL^{-1} isolated mitochondria, 10 μL of 1 M pyruvate/0.5 M Malate and 1μL of 10 mM ADP. See text for discussion.

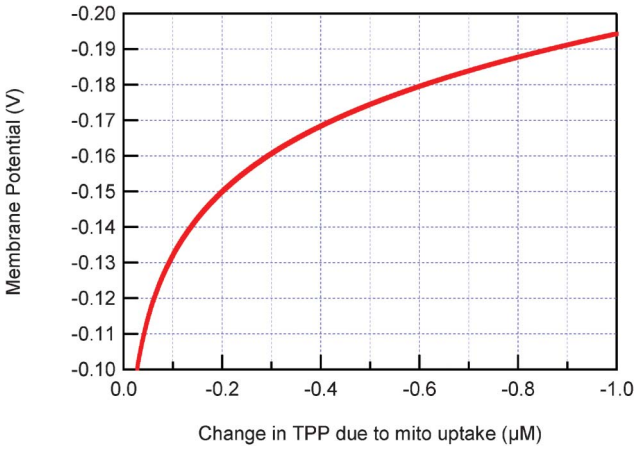

Fig. 4 Conversion of measured $[TPP^+]$ into $\Delta\psi_m$.

due to uptake by the mitochondria. In Fig. 4, we plot the relationship (eq. 1S in supplemental information) of the inferred membrane potential to the measured $[TPP^+]$ concentration change due to the mitochondria $\Delta\psi_m$.

To test functional activities of complex I by adding the OXPHOS substrates, pyruvate and malate (P/M) were added, to stimulate the active shuttling of protons out of the mitochondrial matrix. This resulted in an increase in the magnitude of $\Delta\psi_m$, thus diffusion of TPP^+ into the matrix, resulting in a decrease in $[TPP^+]$ in the medium. Indeed, the response to P/M was instantaneous and stabilized to reveal a drastically decreased $[TPP^+]$ by 1.5 μM in the sensing chamber. Once these data were collected, we wanted to ensure the viability of our mitochondria to validate that the TPP^+ efflux is active and not merely due to defunct OXPHOS machinery, degraded membranes, *etc.* To that end, we added ADP to take advantage of the fact that OXPHOS complex V (ATP synthase) utilizes the $\Delta\psi_m$ to convert ADP to ATP. Accordingly, we detected the increase of TPP^+ ions in the chamber, indicating a partial depolarization of the $\Delta\psi_m$ which was used to drive ATP synthesis. Due to the physical effect of manual injections using a micropipette, signal noise was recorded as scattered data when injections were performed. This could be eliminated by employing an automated fluidic perfusion system in future designs.

The same series of measurements with mitochondria from Heb7A and mouse muscle cell lines were performed and compared. The amount of mitochondria and chemicals as well as the sequence of injections remained the same to avoid variations from assay to assay. Drops of $[TPP^+]$ after addition of mitochondria, and the corresponding $\Delta\psi_m$ values are plotted in Fig. 5 which were obtained from 6 different assays. As expected from prior studies of mitochondrial bioenergetics, $\Delta\psi_m$ of mitochondria from mouse skeletal muscle showed the largest value among other cell lines indicating the vibrant activity of the skeletal muscle tissue. (Run to run variations are attributed to sensor drift, to be discussed below in further detail.) The membrane potential of Heb7A was slightly higher than that of 143b. Overall the results of the mitochondrial assays were consistent with the results of prior studies.[12,14]

We now turn to a detailed error analysis of our procedure. In our experiments, the statistical variation (as a function of time)

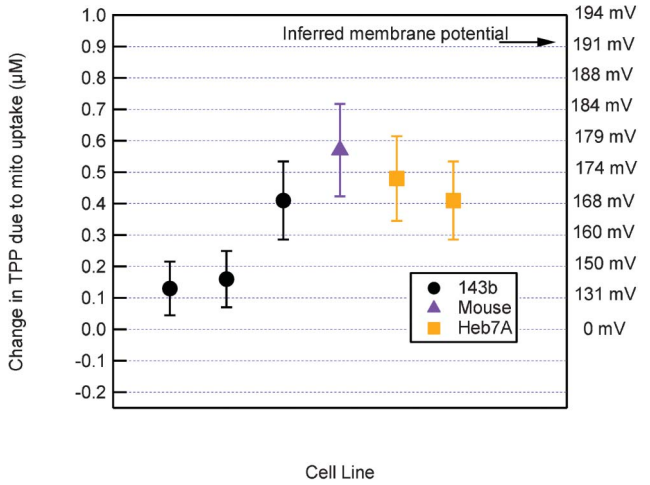

Fig. 5 Data comparisons of drops in [TPP^+] due to mitochondrial uptake measured right after addition of mitochondria. Right axis shows calculated $\Delta\psi_m$ of isolated mitochondria. Data are from three different cell lines (143b, mouse muscle, Heb7A). Error bars are due to calibration uncertainty of the ISE electrode potential to [TPP^+].

when the sensor was stable was quite low. For example, the standard deviation of the measured ISE potential for the time trace shown in Fig. 3 in the stable region between t $\sim$ 500 s and t $\sim$ 600 s is only 50 μV. In this experiment, for this trace, this corresponds to a standard deviation of 0.02 μM in the value of [TPP^+]. The inferred value of $\Delta\psi_m$ has a standard deviation of only 0.5 mV. Each point was integrated for $\sim$ 1 s. (For a 10 ms integration time, this would correspond to a 5 mV standard deviation on the inferred membrane potential.) *This corresponds to an order of magnitude improvement over our first generation technology.*[11] In addition to rapid, random fluctuations due to statistical variations, we also observed permanent, progressive changes in the measured [TPP^+] values, which we attribute to the actual biochemistry of the mitochondria which respond on a much longer time scale compared to the measurement time per point of one second. Since we do not typically observe these long term drifts during calibration without mitochondria (see *e.g.* the inset of Fig. 2 (c)) we believe the time dependent behavior we observe is not due to the sensor technology itself. Indeed, this demonstrates the ability of our technology to assay kinetic as well as equilibrium bioenergetics.

Drift of the calibration during the measurement is more significant, and we address this issue now. In principle, the histograms of Fig. 2 provide a complete quantification of this drift between calibrations and devices. As discussed earlier, it is possible to improve on this error by performing calibrations just before and after the experiment, and using identical conditions in order to compare the behavior between devices. As discussed above, the initial value of [TPP^+] is known accurately, so that the small changes from this initial value can be determined only from small changes in the measured sensor voltage and the (logarithmic) slope (J^{-1}) of the calibration curve, the offset being less important because only small changes about the known, initial value are considered. For the example experiment in Fig. 3, the introduction of mitochondria into the chamber changed the value of [TPP^+] by, at most, 1 μM. Since the initial value is known with low error, and the (logarithmic) slope is determined with a drift of less than 15% during the measurement (worst case, see above), the value of the *change* in the value of [TPP^+] is known to within at worst $\sim$ 0.1 μM. The error bar due to the uncertainty in the slope J is the dominant error, and indicated in Fig. 5. (Note that due to the non-linear relationship between the measured ISE potential and the inferred value of [TPP^+], the error in [TPP^+] gets approximately linearly worse as the *change* in [TPP^+] increases from 0 to 1 μM. We have determined numerically that the error is at most $\pm$ 0.12 μM error for a 1 μM drop in [TPP^+] on introduction of mitochondria, and less for smaller drops in [TPP^+], by calculating [TPP^+] for different values of J^{-1} and determining the worst case error at each value of inferred TPP^+ drop.) In order to relate the calibration drift component of this [TPP^+] error to an error in the inferred value of $\Delta\psi_m$, we use eq. 1S of supplemental information. As can be seen in Fig. 4, this conversion is non-linear, so the error conversion will depend on the specific parameters of the experiment. In our case, this still allows an error smaller than $\sim \pm$ 10 mV for the determination of high values of $\Delta\psi_m$. This error increases as the values of $\Delta\psi_m$ decreases from 180 mV. These parameters will continue to allow studies on the relative value of $\Delta\psi_m$ between different cell lines. This can thus be a powerful tool for the accurate investigation of mitochondrial membrane potential from a variety of cell lines where sample size is limited, such as clinical biopsies or embryonic stem cells.

The sensors developed here remained completely functional for longer than three months and exhibited reproducible responses for over 40 assessments without replacing the TPP^+ ion selective membrane or Ag/AgCl electrodes. For further improvement on sensor performance and the stability, there are three possible avenues. First, a temperature controller to control medium temperature would enable improved stability of the calibration curve and also bioenergetics studies, which are important to carry out at a known (rather than ambient) temperature. Second, an on-chip stirrer could be integrated into the chamber for continuous mixing during the assay. Lastly, a sensor equipped with an automated sample perfusion system with an encapsulated sensing chamber would provide better stability and measurements compared to a manual sample injection by a micropipette.

Conclusions

A wafer-scale fabrication process for a TPP^+ ion selective microsensor for mitochondrial membrane potential assays has been developed and demonstrated. The newly designed process includes the new membrane transfer method which is compatible with microelectronic fabrication techniques resulting in high yield and high throughput process by integrating 6 devices into a single wafer. Further improvement is possible with more effort to increase the number of devices on a single wafer. Due to the improved bonding condition between the TPP^+ ion selective membrane and the bottom PDMS layer, the devices showed structural stability and robustness over an extended period of time (> 3 months) with nominally identical sensitivity to changes in [TPP^+]. Due to the system design, in the future it is feasible to run several assays in parallel at the same time for high throughput studies. This will allow a cost-effective method to mass-produce miniaturized mitochondrial assay chips, which are candidates to replace the current costly systems installed with large, traditional sensing chambers. For these reasons, our system can find various applications in the emerging field of mitochondrial bioenergetics.

Acknowledgements

This work was supported in part by the following grants awarded to D.C.W.: NIH-AG24373, NS21328, AG13154, DK73691, CIRM Comprehensive Grant RC1-00353, and a Doris Duke Clinical Interface Grant 2 005 057. P.B. acknowledges support of this work from NIH National Cancer Institute Grant 1R21CA143351-01, as well as support from the ARO (MURI W911NF-11-1-0024). Antonio Davila is supported by the National Science Foundation Lifechips Integrative Graduate Education and Research Traineeship 0 549 479.

References

1 G. Solaini, *et al.*, "Evaluating mitochondrial membrane potential in cells", *Biosci. Rep.*, 2007, **27**, 11–21.
2 S. P. Apte and R. Sarangarajan, *Cellular Respiration and Carcinogenesis*, Humana Press, Springer, New York City, 2009.
3 G. Kroemer, *et al.*, "Mitochondrial membrane permeabilization in cell death", *Physiol. Rev.*, 2007, **87**, 99–163.
4 L. Galluzzi, *et al.*, "Mitochondria as therapeutic targets for cancer chemotherapy", *Oncogene*, 2006, **25**, 4812–4830.
5 P. Rustin and G. Kroemer, "Mitochondria and Cancer", in *Ernst Shering Foundation Symposium Proceedings*. vol. **4**, Springer-Verlag, Berlin, 2008, pp. 1–21.
6 L. Galluzzi, *et al.*, "Methods to dissect mitochondrial membrane permeabilization in the course of apoptosis", in *Programmed Cell Death, General Principles for Studying Cell Death, Pt A*. vol. **442**: Elsevier Academic Press Inc, San Diego, 2008, pp. 355–374.
7 L. Galluzzi, *et al.*, "Methods for the assessment of mitochondrial membrane permeabilization in apoptosis", *Apoptosis*, 2007, **12**, 803–813.
8 D. C. Wallace, *et al.*, "Mitochondrial Genes in Degenerative Diseases, Cancer and Aging" in *Emery and Rimoin's Principles and Practice of Medical Genetics, 5th Edition*. vol. **1**, Chapter 13, ed. D. L. Rimoin, *et al.*, Churchill Livingstone Elsevier, Philadelphia, PA, 2007, pp. 194–298.
9 D. C. Wallace, "A mitochondrial paradigm of metabolic and degenerative diseases, aging and cancer: A dawn for evolutionary medicine", *FASEB J.*, 2006, **20**, A1474–A1474.
10 D. C. Wallace, A mitochondrial paradigm of metabolic and degenerative diseases, aging and cancer: a dawn for evolutionary medicine, *Annu. Rev. Genet.*, 2005, **39**, 359–407.
11 T. S. Lim, *et al.*, "Assessment of mitochondrial membrane potential using an on-chip microelectrode in a microfluidic device", *Lab Chip*, 2010, **10**, 1683–8.
12 N. Kamo, *et al.*, "Membrane potential of mitochondria measured with an electrode sensitive to tetraphenyl phosphonium and relationship between proton electrochemical potential and phosphorylation potential in steady state", *J. Membr. Biol.*, 1979, **49**, 105–121.
13 A. Labajova, *et al.*, "Evaluation of mitochondrial membrane potential using a computerized device with a tetraphenylphosphonium-selective electrode", *Anal. Biochem.*, 2006, **353**, 37–42.
14 A. Zolkiewska, *et al.*, "Resting state respiration of mitochondria: reappraisal of the role of passive ion fluxes", *Arch. Biochem. Biophys.*, 1989, **275**, 580–90.